processes

MDPI

Article

A Multi-Model Fusion Network for Enhanced Blind Well Lithology Prediction

Xiaoqing Shao [1], Pengwei Zhang [1,*], Shunlai Yan [2], Qing Zhao [3], Yufeng Jia [1], Cheng Zhang [4] and Jun Tian [4]

[1] School of Information Science and Engineering, Xinjiang College of Science & Technology, Korla 841000, China; 2020130@xjust.edu.cn (X.S.); jiayufeng04@126.com (Y.J.)
[2] Geophysical Research Institute, BGP Inc., CNPC, Zhuozhou 072751, China; yanshunlai@cnpc.com.cn
[3] GME & Geochemical Surveys, BGP Inc., CNPC, Zhuozhou 072751, China; zhaoqing02@cnpc.com.cn
[4] China National Petroleum Corporation Tarim Oilfield Branch Company, Korla 841000, China; zhangch6@petrochina.com.cn (C.Z.); tjun-tlm@petrochina.com.cn (J.T.)
* Correspondence: zpw1004@163.com

Abstract: Lithology identification is essential for formation evaluation and reservoir characterization, serving as a fundamental basis for assessing the potential value of oil and gas resources. However, traditional models often struggle with identification accuracy due to the complexities of nonlinear relationships and class imbalances in well-logging data. This paper presents an effective multi-model ensemble approach for lithology identification, integrating one-dimensional multi-scale convolutional neural networks (MCNN1D), Graph Attention Networks (GAT), and Transformer networks. MCNN1D extracts local features of lithological changes with varying convolutional kernels, enhancing robustness to complex geological data. The GAT assigns adaptive weights to adjacent nodes, capturing spatial relationships among lithological samples and enhancing local interactions. Meanwhile, the Transformer uses self-attention to capture contextual relationships in lithological sequences, improving global feature processing and identification. The multi-model fusion effectively combines the strengths of individual models, enabling comprehensive and efficient modeling of geological features. Experimental results show that the proposed Multi-Model Fusion Network outperforms other models in accuracy, precision, recall, and F1-score on the Hugoton–Panoma oilfield dataset, achieving a lithology identification accuracy of 95.06% for adjacent lithologies. This approach mitigates the effects of data imbalance and enhances identification accuracy, making it a powerful tool for lithology identification in complex reservoirs.

Keywords: lithology identification; machine learning; blind well

Academic Editor: Yo-Ping Huang

Received: 15 November 2024
Revised: 2 January 2025
Accepted: 17 January 2025
Published: 20 January 2025

Citation: Shao, X.; Zhang, P.; Yan, S.; Zhao, Q.; Jia, Y.; Zhang, C.; Tian, J. A Multi-Model Fusion Network for Enhanced Blind Well Lithology Prediction. *Processes* **2025**, *13*, 278. https://doi.org/10.3390/pr13010278

1. Introduction

Lithology identification is a fundamental task in petroleum exploration and geological analysis, providing critical insights for reservoir characterization and geological modelling [1–3]. While the analysis of core and cutting samples obtained during drilling is regarded as the most accurate method, it is often costly and time-consuming [4]. Manual specimen identification, thin section analysis, elemental testing, and mineralogical testing can yield detailed information but are limited in practical application due to the considerable workforce and specialized expertise required [5,6]. A "blind well" refers to a well drilled without any prior core samples or geological information [7]. It is typically used to assess the accuracy of predictions concerning rock properties, stratigraphic features, or reservoir characteristics. Adjacent blind wells are oil wells located in similar geographical

areas but with independently distributed logging data, allowing for distinct evaluations within comparable geologic settings [8]. Traditional lithology identification methods, such as cross-plotting, curve feature analysis, and logging imaging, often depend on expert judgment, which can be time-consuming, subjective, and expensive [9,10]. These limitations impede the ability of these methods to meet the increasing demands of modern petroleum exploration and development.

With the increasing availability of logging data and advancements in computer science, machine learning techniques have been widely applied in log interpretation [11]. Machine learning methods can discover correlations between multidimensional data by integrating and learning feature attributes from logging curves. However, traditional machine learning methods often struggle to effectively distribute data, resulting in low accuracy when handling complex, imbalanced multi-label lithology datasets. To overcome these limitations, this study introduces an ensemble approach that integrates MCNN1D, GAT, and Transformer models. This framework is designed to address key challenges such as inter-sample correlation extraction, spatial relationship modeling, and long-range dependency capture. By leveraging the unique strengths of each model, the proposed approach not only improves predictive accuracy but also effectively alleviates the issue of imbalanced lithology data.

2. Related Work

2.1. Machine Learning for Lithology Identification

In recent years, machine learning methods have been extensively applied to lithology identification tasks, significantly enhancing both accuracy and efficiency in this field [12–17]. Liu et al. (2020) developed a multi-kernel support vector machine method combining global and local features, improving accuracy and efficiency in lithofacies identification for complex geological environments [18]. Bressan et al. (2020) evaluated multilayer perceptron, decision tree, random forest, and support vector machine approaches for lithology classification, identifying random forest as the best method [19]. Duan et al. (2020) developed a decision tree method for volcanic rock lithology identification based on logging data from the Laizhouwan Sag in the Bohai Bay Basin, significantly improving classification accuracy [20]. Liu et al. (2024) utilized well logging data from the Chengbei Operation Area of Shengli Oilfield to develop enhanced sampling algorithms combined with a random forest model, significantly improving lithology discrimination under imbalanced sample conditions [21]. Chen et al. (2024) proposed a lithology classification method combining the honey badger optimization algorithm and the extreme gradient boosting tree model, using logging data from the Hongche Fault Zone in the Junggar Basin to achieve high-accuracy volcanic rock identification [22]. Ali et al. (2024) evaluated self-organizing maps, multi-resolution graph-based clustering, k-nearest neighbors, and artificial neural networks for lithofacies identification, finding multi-resolution graph-based clustering to be the most accurate and consistent with core data [23].

2.2. Deep Learning for Lithology Identification

As lithology types become increasingly complex and data distribution imbalances intensify, researchers have increasingly turned to deep learning techniques to tackle the challenges of lithology identification [24–27]. These methods have demonstrated great potential in complex geological environments and under imbalanced data conditions, offering new directions for lithology analysis. Fu et al. (2022) proposed an improved ResNeSt-50 neural network model combined with transfer learning to achieve automatic classification of drill core images. The model achieved an impressive 99.60% accuracy on the test set, providing a reliable and efficient solution for core image classification [28]. Similarly, other

researchers compared well-log data to image data, exploring the potential of convolutional neural networks (CNNs) for feature extraction and prediction. Mousavi and Hosseini-Nasab (2024) introduced a residual convolutional neural network for lithology classification, achieving 93% accuracy and a 79% F1-score using Iranian gas field well-log data [29]. Due to the sequential nature of well-log data, which change with depth and resembles text sequences, researchers have adopted models such as recurrent neural networks (RNNs), long short-term memory (LSTM) networks [30], and gated recurrent units (GRUs) [31] for predictive tasks. Imamverdiyev and Sukhostat (2019) developed a one-dimensional convolutional neural network model (CNN1D) based on well-log data from the Hugoton Basin. By leveraging the Adagrad optimizer, this model efficiently extracted local features, significantly improving lithology classification accuracy and F1-scores compared to traditional methods such as support vector machines (SVMs), k-nearest neighbors (KNNs), RNNs, and LSTM [32]. To address challenges posed by imbalanced data distributions and complex lithology characteristics, researchers have explored more advanced deep learning models. For instance, graph neural networks (GNNs) have gained attention for their ability to capture spatial relationships between samples [33,34]. Traditional graph convolutional networks (GCNs) model well log data as graph structures, effectively extracting spatial dependencies. However, GCN faces limitations in reflecting the importance of individual nodes, which constrains their performance. To overcome this, Yuan et al. (2022) proposed graph attention networks (GATs), which use adaptive attention mechanisms to assign weights to node interactions, precisely capturing inter-node relationships and improving predictions for minority classes [35]. Zhao et al. (2025) further introduced a Residual Graph Attention Network (ResGAT), achieving notable improvements in minority class accuracy [36]. Meanwhile, Transformer models have demonstrated exceptional capabilities in handling sequential data, particularly in capturing long-range dependencies through self-attention mechanisms. Compared to GNNs, Transformers excel in extracting long-distance feature associations from depth-varying well log data, making them particularly effective for sequence-based feature modeling. Sun et al. (2024) proposed a recurrent Transformer model combining recursive structures with multi-scale attention mechanisms, achieving an impressive 97.97% accuracy in lithology identification using well log data from the Tarim Basin. Similarly, Xie et al. (2024) developed a Transformer–LSTM hybrid model for blind well lithology prediction, achieving 88% precision and 89% recall by effectively capturing spatiotemporal features along the depth dimension [37]. In lithology identification tasks, MCNN1D, GAT, and Transformer each demonstrate unique strengths. MCNN1D excels in capturing multi-scale information, providing a more comprehensive understanding of intricate data features. GAT leverages graph-based architectures to effectively model complex inter-sample relationships and spatial dependencies. Meanwhile, Transformer stands out with its exceptional ability to capture long-range dependencies, making it particularly effective for handling sequential and depth-structured data. This study introduces an ensemble learning framework that integrates MCNN1D, GAT, and Transformer models. By harnessing the unique strengths of each model, the framework effectively tackles key challenges, including inter-sample correlation extraction, spatial relationship modeling, and long-range dependency capture. This approach not only significantly enhances the overall accuracy of lithology identification but also mitigates issues related to data imbalance.

3. Methodology

An ensemble method is proposed to improve prediction accuracy and mitigate the impact of data imbalance by integrating MCNN1D, GAT, and Transformer models within a integrated framework, as illustrated in Figure 1. MCNN1D first extracts multi-scale local features (Feature1) from well-log data, Transformer captures contextual relationships

in lithological sequences to extract global features (Feature2), and GAT models spatial relationships between lithological samples to generate Feature3. These features are concatenated and passed through a fully connected (FC) layer, with the final lithology predictions visualized through a Softmax layer. In this study, each data point represents the physical properties at a specific depth within a well, forming a well-logging dataset $\{(x_i, y_i)\}_{i=1}^{n}$ with n samples. x_i is a d-dimensional vector $v = (v_1, v_2, \ldots, v_d)$ in hyperspace, where each scalar component v_i corresponds to a physical property measured by wireline logging, such as gamma-ray (GR), resistivity ($\log_{10}$ ILD), and average neutron-density porosity (PHIND), etc. The label y_i denotes the lithology category of the i-th sample.

For the implementation, we selected datasets from the Hugoton and Panoma gas fields in the USA as examples. Each feature vector x_i has 7 dimensions. The dataset includes data from 10 wells, used as the training set, and data from 2 additional wells, used as blind wells. These blind wells were input into the ensemble model for lithology prediction. The lithology categories are divided into 9 classes.

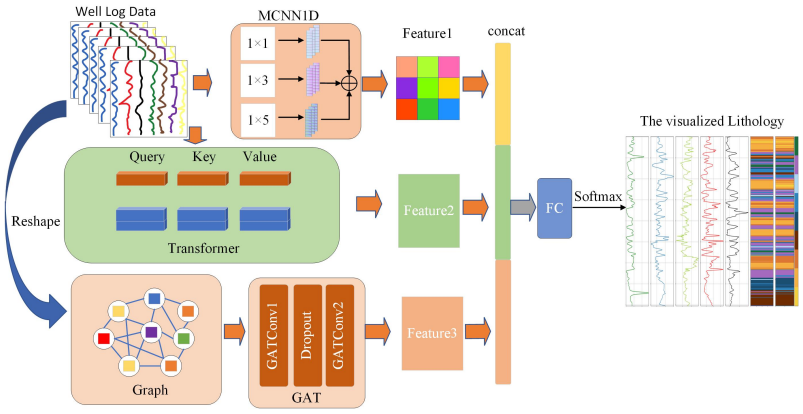

Figure 1. Architecture of the proposed hybrid model for lithology identification using MCNN1D, GAT, and Transformer.

3.1. Data Preprocessing

Before well-log data are used for lithology classification, preprocessing is performed to remove rows with missing values, updating the dataset accordingly. Subsequently, normalization is applied after vectorization to map the values of different logging curves to a range of 0–1 through min–max normalization (see Equation (1)). This normalization process ensures that different features are compared on the same scale, preventing certain features with larger value ranges from dominating the model's training [38,39].

$$X_{\text{norm}} = \frac{X - X_{\text{min}}}{X_{\text{max}} - X_{\text{min}}} \tag{1}$$

In this equation, X_{norm} refers to the standardized attribute value, while X indicates the initial attribute value before normalization. The values X_{min} and X_{max} correspond to the minimum and maximum limits of a specific attribute within a given well-logging curve.

3.2. MCNN1D

By utilizing a series of convolutional kernels of varying scales to extract multi-level features from lithological data, the model can simultaneously understand and capture both the microscopic details and macroscopic structures of the lithological data, enhancing its ability to recognize complex geological formations. The multi-scale selection allows the model to adapt to features at different resolutions within geological layers, improving its

capacity to discern fine-grained details and broader contextual information, ultimately boosting prediction accuracy [40]. This approach is mathematically represented as follows:

$$F_i = \text{Conv1D}(j_i)(X), \quad i = 1, 2, 3, \quad j_i \in \{1, 3, 5\} \tag{2}$$

In this context, F_i represents the feature map obtained using a convolution kernel size of j_i, while $\text{Conv}(j_i)$ denotes the convolution operation. X is the input feature map, and each j_i corresponds to a specific kernel size, specifically $1 \times 1, 1 \times 3$, and 1×5. The MCNN1D model leverages the introduction of multi-scale convolutional kernels to capture both local details and global patterns in geological data simultaneously. Specifically, smaller kernels ($j_1 = 1$) excel at detecting subtle variations in lithological features, medium-sized kernels ($j_2 = 3$) focus on modeling intermediate structures, and larger kernels ($j_3 = 5$) effectively capture broader patterns across geological layers. This multi-scale design enhances the model's adaptability to diverse feature resolutions, making it particularly effective in identifying complex lithological structures.

3.3. GAT

GAT incorporates a self-attention mechanism that adaptively assigns different weights to each node in the graph, effectively capturing relationships between nodes [41,42]. The GAT formula is presented in Equation (3).

$$h_i' = \sigma\left(\sum_{j \in \mathcal{N}(i)} \alpha_{ij} W h_j\right) \tag{3}$$

h_i' denotes the updated feature representation of node i, $\mathcal{N}(i)$ is the set of neighboring nodes of node i, W represents the learnable linear transformation matrix, α_{ij} is the attention weight between node i and its neighboring node j, and σ is the non-linear activation function.

After preprocessing, the lithology data are reshaped, with each well-log sample treated as a node in the lithology identification graph. Edges are established based on the Euclidean distance between node features, connecting nodes within a suitable threshold. Specifically, the Euclidean distance [43] between node i and node j is defined as shown in Equation (4). Adaptively assigning different attention weights to each edge enhances the model's capture of complex relationships.

$$D_{ij} = \sum_{k=1}^{d} (x_{i,k} - x_{j,k})^2 \tag{4}$$

where $x_{i,k}$ denotes the value of node i in the k-th feature; d represents the number of features. An edge is established between nodes i and j if D_{ij} is less than a given threshold T and is not equal to 0. The set of edges E can be represented as shown in Equation (5).

$$E = \{(i, j) \mid 0 < D_{ij} < T\} \tag{5}$$

This self-attention mechanism, as shown in Equation (3), allows GAT to dynamically allocate attention weights to the most relevant neighboring nodes, effectively modeling intricate inter-node dependencies in lithological data. Combined with the graph construction process outlined in Equations (4) and (5), this enables GAT to handle imbalanced lithological datasets more effectively, improving its adaptability and classification accuracy compared to traditional models like GCNs.

3.4. Transformer

The Transformer model is a deep learning architecture based on the attention mechanism, initially applied in natural language processing and now widely adopted across various fields [44]. Within the Transformer model, the multi-head attention mechanism is a pivotal component. The core idea of multi-head attention is to compute attention in parallel across multiple independent "heads", with each head corresponding to a different subspace. This allows the model to analyze distinct features from multiple perspectives rather than being confined to a single viewpoint [45]. Specifically, the model calculates attention weights separately for each head using the Query, Key, and Value matrices, then combines these independent attention outputs to form a richer feature representation. This approach enables the model to simultaneously focus on fine-grained features within lithological data, providing a comprehensive understanding of variations across depths and geological layers. Consider a given lithological data input matrix ($X \in \mathbb{R}^{n\times 7}$), where the 7 represents the features of Hugoton–Panoma lithological data. The input matrix X undergoes a linear transformation to generate the query matrix Q, the key matrix K, and the value matrix V, as shown in Equation (6). The mathematical formulation of the multi-head attention mechanism is provided in Equation (7).

$$Q = XW_Q, K = XW_K, V = XW_V \tag{6}$$

where W_Q, W_K, and W_V are the learnable weight matrices. For each head i , compute the single-head attention as follows:

$$head_i = Attention(Q_i, K_i, V_i) = softmax\left(\frac{Q_i K_i^T}{\sqrt{d_k}}\right)V_i \tag{7}$$

Q_i, K_i and V_i are the query, key, and value matrices for the i-th head, and d_k is the dimensionality of the key vectors. Concatenate the outputs of all the heads:

$$MultiHead(Q, K, V) = Concat(\text{head}_1, \ldots, head_h)W_O \tag{8}$$

where W_O is the linear transformation matrix applied to the concatenated output. The multi-head attention mechanism adeptly captures intricate dependencies and patterns within geological data, facilitating a more precise and nuanced comprehension of subsurface formations.

The Transformer model demonstrates good performance in lithology identification due to its ability to simultaneously capture local details and global dependencies within geological data. The multi-head attention mechanism allows the model to process fine-grained lithological features while retaining an understanding of broader subsurface patterns. This characteristic is particularly useful when dealing with complex subsurface formations or imbalanced data distributions, where certain traditional models may face challenges. Additionally, the flexibility of the Transformer architecture enables it to adapt to different resolutions and feature representations, offering a practical solution for geological applications.

4. Data and Model Settings

4.1. Data Overview

The Hugoton and Panoma fields, located in Kansas, USA, are among the most significant natural gas-producing regions in the country [46]. These fields feature complex geology, primarily sandstone and limestone, and are rich in natural gas and oil resources. This study utilized 4979 log data points from twelve wells in these fields for experimentation. The wells named STUART and CRAWFORD were used as blind wells to predict

reservoir lithology. The well-logs from these drillings encompass various parameters: Gamma Ray (GR) is used to measure the natural radioactivity in rocks and is commonly employed to identify clay content, as clay minerals typically exhibit higher radioactivity. Deep Induction Log (ILD_log10), which utilizes logarithmic scaling, measures the resistivity of formations, aiding in the analysis of resistivity variations at different depths; high resistivity is often associated with low porosity or hydrocarbon saturation. The Photoelectric Effect (PE) measures the photoelectric absorption cross-section of rocks, which is directly related to their density and composition, making it particularly suitable for distinguishing between carbonate rocks and sandstones. Neutron Density Porosity Difference (DeltaPHI) represents the difference between neutron and density porosities, indicating changes in fluid type and rock properties. Average Neutron Density Porosity (PHIND) is calculated using neutron and density log data to evaluate the reservoir quality of formations. The Nonmarine–Marine Indicator (NM_M) is used to differentiate between marine and nonmarine depositional environments, assisting in identifying and interpreting geological history and its impacts. Relative Position (RELPOS) denotes the relative depth position of a point within the entire logging curve, helping to standardize the data for easier comparison and analysis. These parameters provide crucial insights into formation structure, rock properties, and potential hydrocarbon content.

The lithology types include marine siltstone and shale (SiSH), nonmarine sandstone (SS), nonmarine coarse siltstone (CSiS), nonmarine fine siltstone (FSiS), dolomite (D), mudstone (MS), wackestone (WS), packstone–grainstone (PS), and phylloid-algal bafflestone (BS).

Due to the continuity and similarity of rock properties, certain lithology types are geologically close and are referred to as "adjacent lithologies". These types share similar characteristics, making them more prone to misclassification or confusion during categorization or prediction tasks. For example, Zhao et al. conducted a study based on logging datasets from the Hugoton and Panoma fields in Kansas, USA, and presented the adjacent relationships between different lithology types in a clear and intuitive tabular format [8].

In lithology identification research, scatter plot matrices effectively illustrate relationships between various logging variables (e.g., GR, PE, ILD_log10, DeltaPHI, and PHIND) within the Hugoton–Panoma dataset (see Figure 2). Different colors represent distinct lithology types, providing a visual means to reveal variations and potential associations in the distributions of each lithology. In Figure 2, the scatter plots of logging variables show substantial overlap among different lithology types, indicating similar distribution patterns and unclear boundaries between classes. This overlap increases classification difficulty, as the model may struggle to identify distinct features for each lithology, leading to a higher risk of misclassification.

To present high-dimensional samples more intuitively, we applied t-SNE to reduce the data to a three-dimensional space, with the visualization results shown in Figure 3. The distribution of lithofacies categories in the Hugoton–Panoma dataset, as shown in Figure 4, reveals a significant class imbalance. Categories like CSiS and FSiS have the highest counts, while BS and D are comparatively less represented. This indicates that the region's lithology is characterized by category imbalance and multi-label complexity, with indistinct boundaries and excessive proximity between different lithologies, making it challenging to differentiate them.

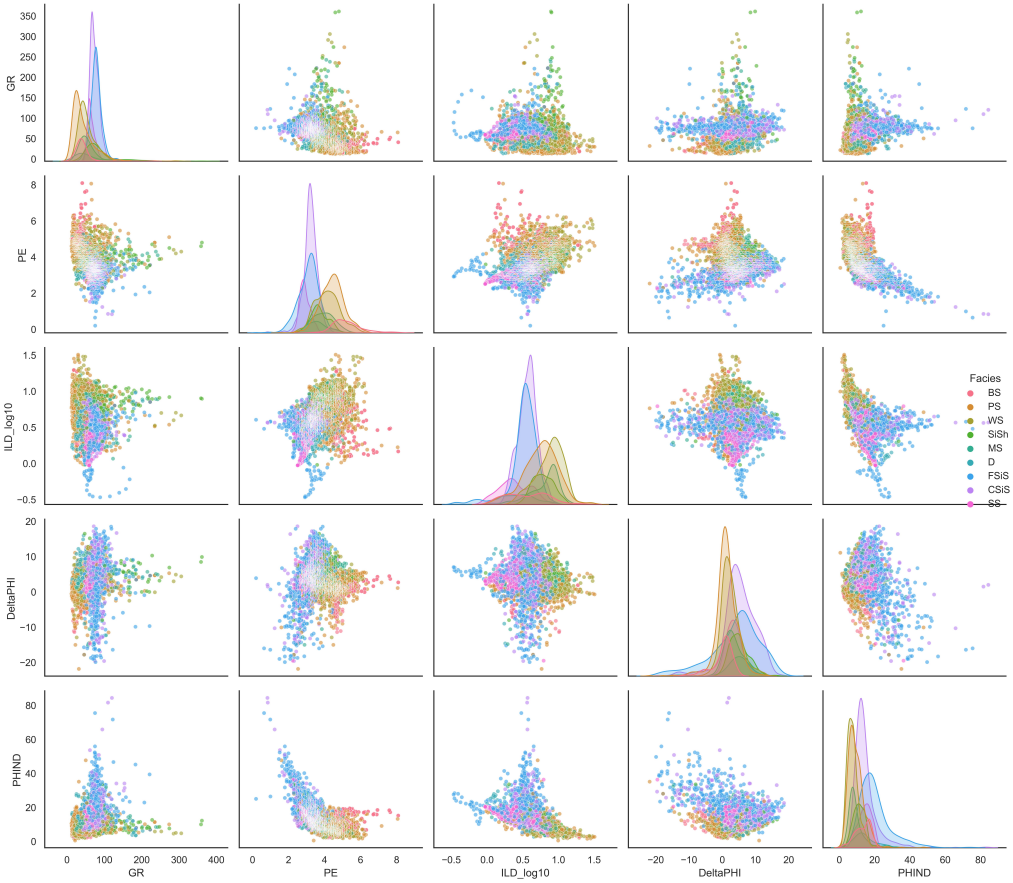

Figure 2. Scatter plot matrix of logging variables for lithology types in the Hugoton–Panoma dataset.

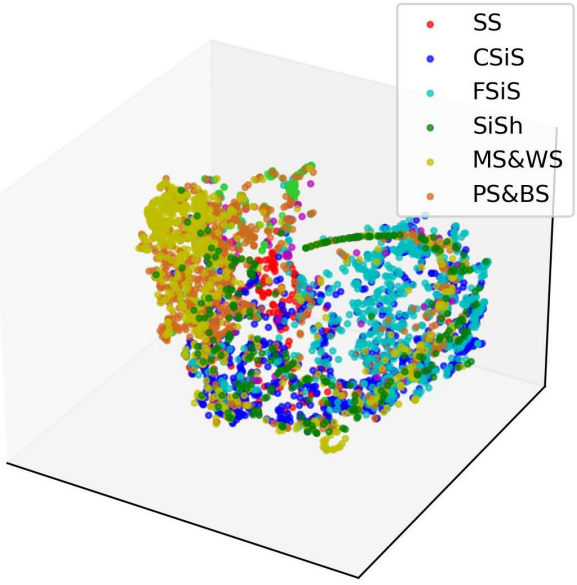

Figure 3. 3D t-SNE Visualization of lithology types in the dataset.

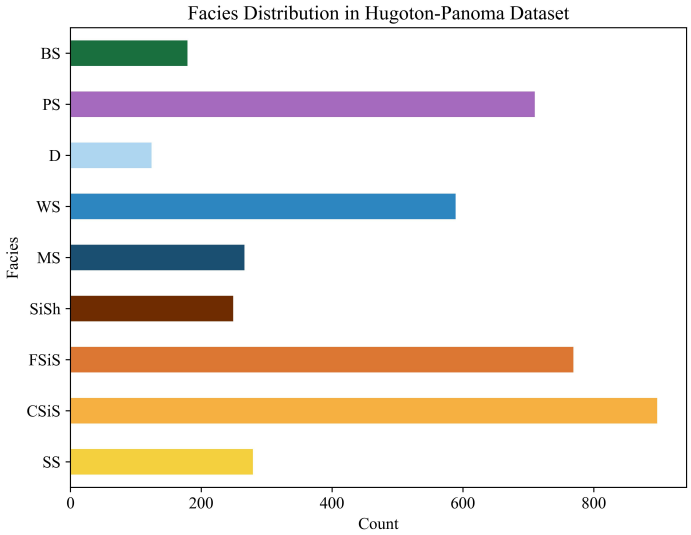

Figure 4. Distribution of lithology types in the Hugoton–Panoma dataset.

4.2. Model Settings

The feature vectors generated by the MCNN1D, GAT, and Transformer modules are concatenated and fused before being passed into a fully connected layer (FC). This fusion strategy harnesses the unique strengths and distinct characteristics of each model component, creating a richer and more comprehensive feature representation. The training process utilizes the Adam optimizer with a learning rate of 0.002 and optimizes using the CrossEntropyLoss function. The model is trained over 400 epochs to maximize its performance across the dataset, leveraging the complementary insights provided by each module, as detailed in Table 1.

Table 1. Configuration details for each model component.

Component	Layer Type	Configuration Details
GAT	Graph Attention Layer 1	Input size: 7; Hidden size: 128; Heads: 8; Dropout: 0
	Graph Attention Layer 2	Hidden size: 1024; Heads: 1
	Activation	ReLU
MCNN1D	Convolutional Layer 1	In channels: 1; Out channels; 32, Kernel size; 1, Padding: 0
	Convolutional Layer 2	In channels: 1; Out channels: 32; Kernel size: 3; Padding: 1
	Convolutional Layer 3	In channels: 1; Out channels: 32; Kernel size: 5; Padding: 2
	Linear Layer	Input size: 672; Output size: 128
	Activation	ReLU
Transformer	Linear Layer (Input)	Input size: 7; Hidden size: 128
	Transformer Encoder	d_model: 128; Heads: 2; Layers: 1; Dropout: 0.5
	Layer Normalization	Hidden size: 128
	Linear Layer (Output)	Output size: 128
	Activation	ReLU
	Dropout	Rate: 0.5

The hyperparameter selection in this study was based on both a literature review and grid search results. For instance, the ReLU activation function was chosen for its efficiency, while the Adam optimizer was selected for its ability to handle sparse gradients and achieve fast convergence. The learning rate (0.002) was determined through grid search and validation. The input size and hidden layer size were set based on the feature dimensions of the Hugoton–Panoma dataset and further refined through experimentation.

Additionally, the CrossEntropy loss function was utilized for its effectiveness in multi-class classification tasks.

5. Results

5.1. Model Evaluation Criteria

In the experiments, accuracy, precision, recall, and F1-score are used to evaluate model performance. Accuracy indicates the overall correct classification rate (refer to Equation (9)), precision assesses the accuracy of positive predictions (as defined in Equation (10)), and recall reflects the model's sensitivity (outlined in Equation (11)). The F1-score, calculated as the harmonic mean of precision and recall (detailed in Equation (12)), provides a balanced measure of performance.

$$\text{Accuracy} = \frac{TP + TN}{TP + TN + FP + FN} \tag{9}$$

$$\text{Precision} = \frac{TP}{TP + FP} \tag{10}$$

$$\text{Recall} = \frac{TP}{TP + FN} \tag{11}$$

$$\text{F1 Score} = \frac{2 \cdot \text{Precision} \cdot \text{Recall}}{\text{Precision} + \text{Recall}} \tag{12}$$

5.2. Comparison on Adjacent Blind Wells

In this study, we selected ten wells from the Hugoton–Panoma dataset to construct the training set, leveraging the diverse logging profiles of these wells to capture the variability in lithology and other geological characteristics. To evaluate the generalizability and accuracy of the proposed model, two wells (STUART and CRAWFORD) were designated as blind wells. These blind wells were excluded from the training process, enabling a rigorous assessment of the model's performance on unseen data. Incorporating blind wells as test cases allows us to quantify the model's predictive accuracy in practical scenarios, affirming its potential application across neighboring wells. This setup replicates real-world conditions where a model trained on known wells is applied to predict characteristics in newly encountered, adjacent wells.

The experimental results, shown in Table 2, demonstrate that the proposed multi-model fusion approach significantly outperforms other baseline models in terms of accuracy, precision, recall, and F1-score. On the Hugoton–Panoma dataset, the proposed model achieved an accuracy of 70.12%, a precision of 74.27%, a recall of 70.12%, and an F1-score of 70.42%. Compared to single models such as Transformer, MCNN1D, or GAT, as well as traditional machine learning methods like SVM and Random Forest, the proposed model exhibits comprehensive performance improvements. These results highlight the model's ability to more accurately identify lithology types across different wells and effectively capture the complexity of their geological attributes.

If similar lithologies are grouped into the same category based on the adjacent lithology relationships described in previous studies, the trends in training accuracy for lithology and adjacent lithology, as demonstrated by the model proposed in this paper, are shown in Figure 5. After 400 training epochs, the accuracy for adjacent lithology reaches 95.06%.

Table 2. Performance comparison of machine learning models for lithology identification on the Hugoton–Panoma dataset.

Model	Accuracy (%)	Precision (%)	Recall (%)	F1-Score (%)
SVM	56.51	62.21	56.51	53.77
Decision Tree	56.39	61.96	56.39	56.89
XGBoost	63.25	67.08	63.25	63.14
AdaBoost	56.99	61.22	56.99	58.17
Random Forest	66.02	69.69	66.02	65.52
Transformer	68.67	71.74	68.67	67.41
GCN	61.45	64.67	61.45	60.14
GAT	67.47	69.48	67.47	66.97
MCNN1D	68.92	73.11	68.92	69.29
LSTM	68.55	72.22	68.55	68.67
GRU	68.31	72.08	68.31	68.96
Ours	**70.12**	**74.27**	**70.12**	**70.42**

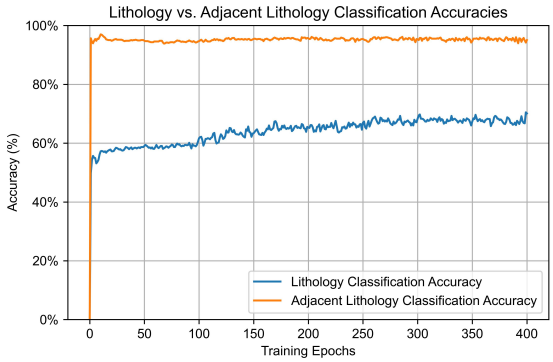

Figure 5. Trends in training accuracy for lithology and adjacent lithology classification.

Figures 6 and 7 present the visualization results of lithology prediction for blind wells in the Hugoton–Panoma dataset based on the proposed Multi-Model Fusion Network. These visualizations compare the predicted lithofacies (right) with the actual lithofacies (left), clearly demonstrating the model's reasonable performance in lithology identification across various depths.

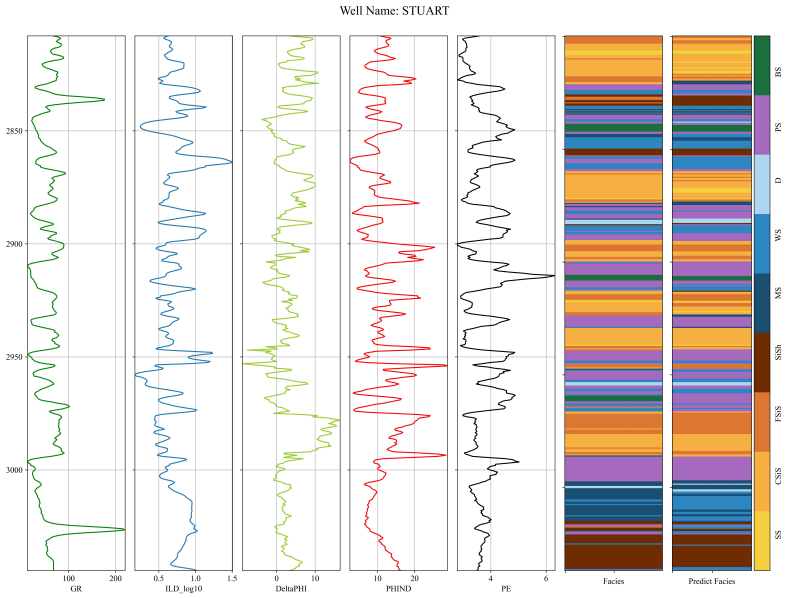

Figure 6. The visualisation of blind lithology identification results for well STUART.

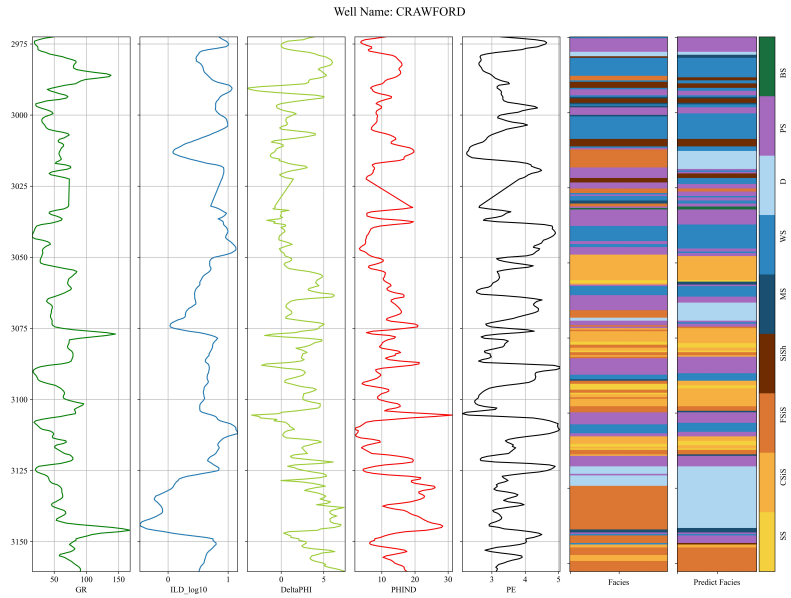

Figure 7. The visualisation of blind lithology identification for well CRAWFORD.

6. Discussion

This study proposes a multi-model fusion network leveraging the strengths of MCNN1D, GAT, and Transformer. MCNN1D extracts local and global features, GAT models spatial dependencies to detect subtle lithological variations, and Transformer captures sequential patterns to enhance classification of complex lithologies. The confusion matrices (Figures 8–11) clearly illustrate the performance improvements achieved by the proposed method on the Hugoton–Panoma dataset, validating its effectiveness in lithology identification tasks. Compared to traditional machine learning models such as SVM and Random Forest, as well as standalone models like MCNN1D, GAT, or Transformer, the proposed multi-model fusion approach demonstrates significant advancements across key metrics, including accuracy, precision, recall, and F1-score. Notably, the model excels in identifying minority lithology classes, a strength attributed to its integration of multi-scale convolutional layers, graph attention mechanisms, and Transformer-based architecture. Furthermore, as illustrated in Figures 8–11, all models tend to frequently misclassify FSiS as D, while rarely misclassifying D as FSiS. This asymmetrical misclassification pattern is likely attributed to feature overlap and class imbalance. To address this issue, future research could leverage geological prior knowledge (e.g., depositional sequences or adjacency relationships) and implement attention mechanisms or a two-stage classification framework to enhance classification accuracy and minimize misclassification.

Although the proposed method excels in improving the accuracy of minority class identification, several limitations remain that warrant further attention. First, the reliance on a single data source may constrain the model's generalizability and adaptability to different geological environments. Incorporating diverse data sources, such as well-logs from multiple oilfields, could significantly enhance the model's robustness and applicability. Furthermore, the model's performance under high-data-diversity scenarios requires further optimization, which is crucial for broader application in complex geological settings. Second, the computational complexity of the ensemble framework poses challenges for deployment in resource-constrained environments. Addressing this issue could involve exploring model compression techniques such as pruning and quantization to reduce parameter size and computational demands. Optimizing the framework design to minimize computational redundancy and resource consumption, as well as developing lightweight sub-models tailored for resource-limited environments, could substantially reduce complex-

ity while maintaining predictive accuracy. Finally, enhancing the model's robustness and adaptability remains a key area for future research. Addressing class imbalance through advanced data augmentation techniques (e.g., SMOTE and GAN) and utilizing transfer learning to improve generalization across diverse geological environments will allow the model to adapt more effectively to complex and varied data distributions. These optimization strategies are expected to address the challenges of computational complexity and significantly enhance the model's practical applicability across various geological scenarios, providing more substantial support for lithology identification tasks.

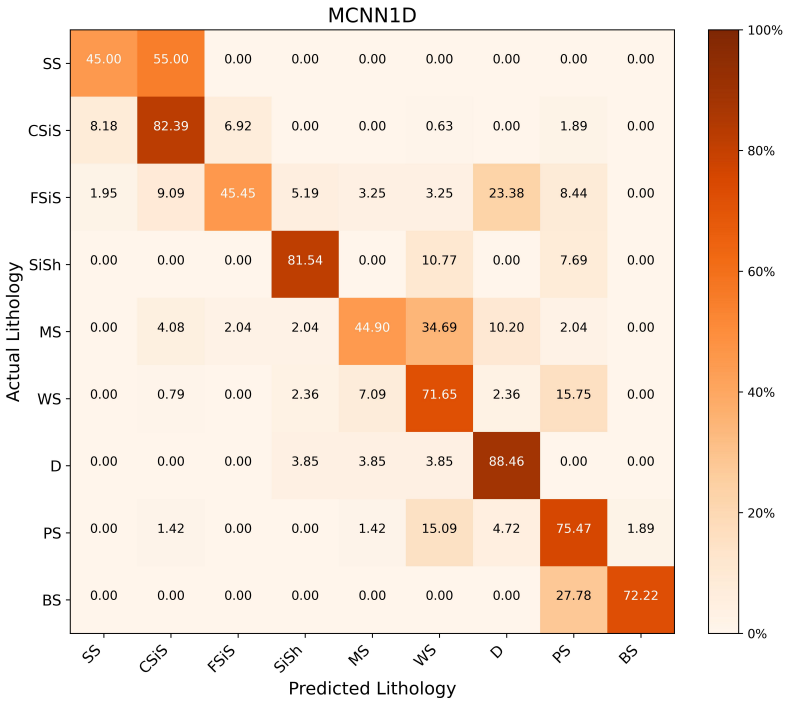

Figure 8. Confusion matrix for lithology identification using MCNN1D.

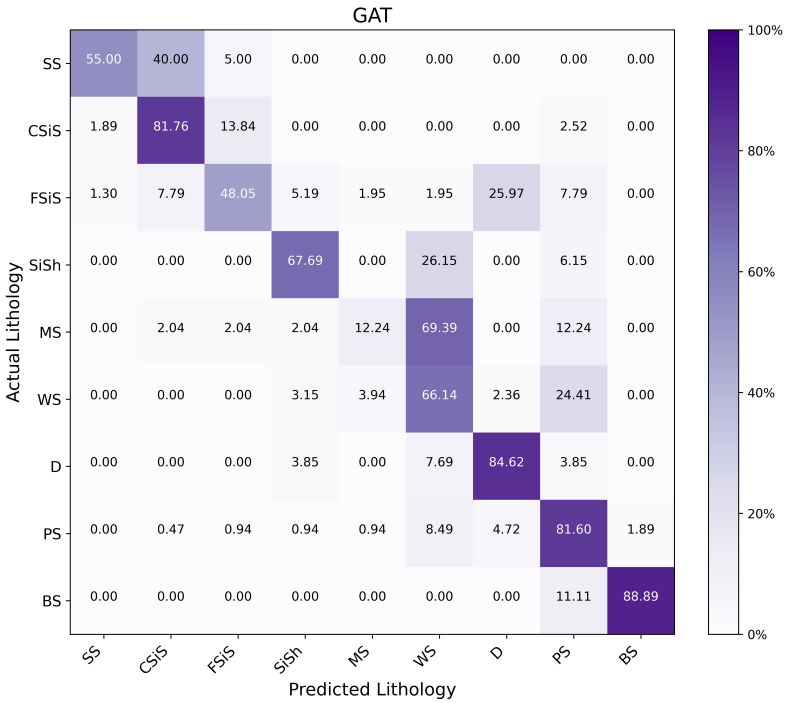

Figure 9. Confusion matrix for lithology identification using GAT.

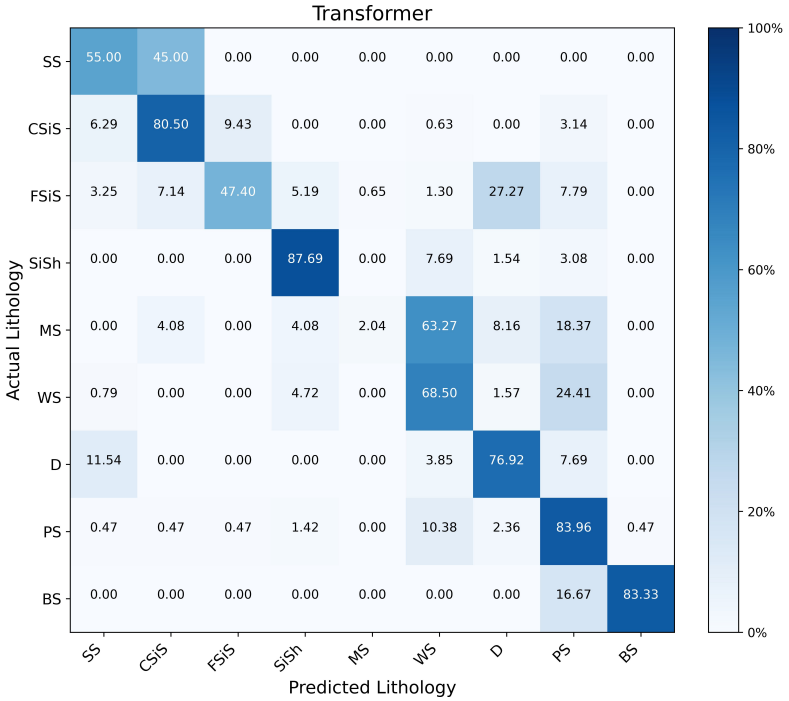

Figure 10. Confusion matrix for lithology identification using Transformer encoder.

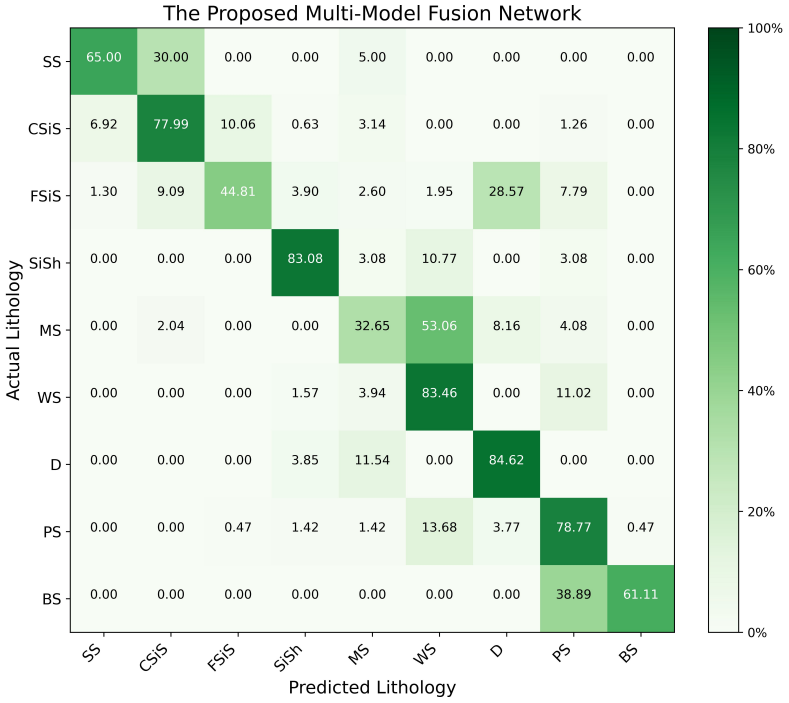

Figure 11. Confusion matrix for lithology identification using the proposed model.

7. Conclusions

This study proposed a multi-model fusion network that combines MCNN1D, GAT, and Transformer to improve lithology identification. The model addresses challenges such as class imbalance, feature overlap, and adjacent lithology misclassification by integrating multi-scale feature extraction, spatial dependency modelling, and sequential pattern learning. Experimental results on the Hugoton–Panoma dataset indicate that the model performs well in blind well predictions (e.g., STUART and CRAWFORD) and demonstrates improvements in accuracy and minority lithology identification compared to traditional methods, highlighting its potential for practical geological applications. However, some

limitations remain. Reliance on a single dataset may affect the model's generalizability, and future work could incorporate more diverse geological datasets to improve robustness. Additionally, the model's computational complexity poses challenges for deployment in resource-constrained environments, which could be addressed through model compression and optimization techniques. Leveraging geological prior knowledge and advanced data augmentation strategies may further enhance the model's adaptability to complex geological conditions. In the future, we aim to optimize the model architecture further and explore its application in other well-log interpretation tasks, such as porosity, permeability, and hydrocarbon saturation predictions, thereby extending its utility in geological data analysis.

Author Contributions: Conceptualization, X.S.; methodology, X.S.; writing—original draft, X.S.; conceptualization, P.Z.; validation, P.Z.; writing—review and editing, P.Z.; resources, S.Y.; data curation, S.Y.; visualization, Q.Z.; investigation, Q.Z.; software, Y.J.; visualization, C.Z.; validation, J.T. All authors have read and agreed to the published version of the manuscript.

Funding: This work was supported in part by the Xinjiang Uygur Autonomous Region University Scientific Research Project (Key Natural Science Project), China Grant No. XJEDU2021I029, Key Talent Training Program of Xinjiang College of Science & Technology (2024-GGYX02), and Xinjiang College of Science & Technology Research Fund (2024-KYPT31).

Data Availability Statement: The data are available on request from the authors.

Acknowledgments: We sincerely appreciate all team members who contributed to this project and the journal editors and reviewers whose insightful feedback significantly enhanced the quality of this paper.

Conflicts of Interest: Authors Shunlai Yan, Qing Zhao, Cheng Zhang and Jun Tian were employed by the company CNPC. The remaining authors declare that the research was conducted in the absence of any commercial or financial relationships that could be construed as a potential conflict of interest. The CNPC had no role in the design of the study; in the collection, analyses, or interpretation of data; in the writing of the manuscript, or in the decision to publish the results.

Abbreviations

CNN	Convolutinal Neural Networks
MCNN1D	Multi-Scale One-Dimensional Convolutional Neural Network
GAT	Graph Attention Network
SVM	Support Vector Machine
Decision Tree	DT
XGBoost	EXtreme Gradient Boosting
RNNs	Recurrent Neural Networks
LSTM	Long Short-Term Memory
GRU	Gated Recurrent Unit
AdaBoost	Adaptive Boosting
RF	Random Forest
K-Nearest Neighbour	KNN
Artificial Neural Networks	ANNs
SS	Nonmarine Sandstone
CSiS	Nonmarine Coarse Siltstone
FSiS	Nonmarine Fine Siltstone
SiSH	Marine Siltstone and Shale
MS	Mudstone
WS	Wackestone
D	Dolomite
PS	Packstone–Grainstone
BS	Phylloid-Algal Bafflestone

References

1. Sun, Z.; Jiang, B.; Li, X.; Li, J.; Xiao, K. A Data-Driven Approach for Lithology Identification Based on Parameter-Optimized Ensemble Learning. *Energies* **2020**, *13*, 3903. [CrossRef]
2. Yan, T.; Xu, R.; Sun, S.H.; Hou, Z.K.; Feng, J.Y. A Real-Time Intelligent Lithology Identification Method Based on a Dynamic Felling Strategy Weighted Random Forest Algorithm. *Pet. Sci.* **2024**, *21*, 1135–1148. [CrossRef]
3. Shi, H.; Xu, Z.; Lin, P.; Ma, W. Refined Lithology Identification: Methodology, Challenges and Prospects. *Geoenergy Sci. Eng.* **2023**, *231*, 212382. [CrossRef]
4. Ao, Y.; Zhu, L.; Guo, S.; Yang, Z. Probabilistic Logging Lithology Characterization with Random Forest Probability Estimation. *Comput. Geosci.* **2020**, *144*, 104556. [CrossRef]
5. Jiang, C.; Zhang, D.; Chen, S. Lithology Identification from Well-Log Curves via Neural Networks with Additional Geologic Constraint. *Geophysics* **2021**, *86*, IM85–IM100. [CrossRef]
6. Zhang, P.; Ren, J.; Zhao, F.; Li, X.; He, H.; Jia, Y.; Shao, X. MS-CGAN: Fusion of Conditional Generative Adversarial Networks and Multi-Scale Spatio-Temporal Features for Lithology Identification. *J. Appl. Geophys.* **2024**, *230*, 105531. [CrossRef]
7. Xie, D.; Liu, Z.; Wang, F.; Song, Z. A Transformer and LSTM-based Approach for Blind Well Lithology Prediction. *Symmetry* **2024**, *16*, 616. [CrossRef]
8. Zhao, F.; Yang, Y.; Kang, J.; Li, X. CE-SGAN: Classification Enhancement Semi-Supervised Generative Adversarial Network for Lithology Identification. *Geoenergy Sci. Eng.* **2023**, *223*, 211562. [CrossRef]
9. Liu, M.; Hu, S.; Zhang, J.; Zou, Y. Methods for Identifying Complex Lithologies from Log Data Based on Machine Learning. *Unconv. Resour.* **2023**, *3*, 20–29. [CrossRef]
10. Liu, J.; Guo, K.; Zhang, S.; Gao, X.; Liu, J.; Li, Q. Identification of Multi-Parameter Fluid in Igneous Rock Reservoir Logging—A Case Study of PL9-1 in Bohai Oilfield. *Processes* **2024**, *12*, 1537. [CrossRef]
11. Jamshidi Gohari, M.S.; Emami Niri, M.; Sadeghnejad, S.; Ghiasi-Freez, J. An Ensemble-Based Machine Learning Solution for Imbalanced Multiclass Dataset during Lithology Log Generation. *Sci. Rep.* **2023**, *13*, 21622. [CrossRef] [PubMed]
12. Zhang, Z.; Fang, S.; Shen, W. Lithology Identification by Support Vector Machine Using Well Logging Data. In Proceedings of the International Workshop on Environment and Geoscience, Hangzhou, China, 15–17 June 2018; pp. 400–405. [CrossRef]
13. Wang, X.; Yang, S.; Zhao, Y.; Wang, Y. Lithology Identification Using an Optimized KNN Clustering Method Based on Entropy-Weighed Cosine Distance in Mesozoic Strata of Gaoqing Field, Jiyang Depression. *J. Pet. Sci. Eng.* **2018**, *166*, 157–174. [CrossRef]
14. Pratama, H. Machine Learning: Using Optimized KNN (K-Nearest Neighbors) to Predict the Facies Classifications. In Proceedings of the 13th SEGJ International Symposium, Tokyo, Japan, 12–14 November 2018; Society of Exploration Geophysicists and Society of Exploration Geophysicists of Japan: Tokyo, Japan, 2019; pp. 538–541. [CrossRef]
15. Ruiyi, H.; Zhuwen, W.; Wenhua, W.; Fanghui, X.; Xinghua, Q.; Yitong, C. Lithology Identification of Igneous Rocks Based on XGboost and Conventional Logging Curves, a Case Study of the Eastern Depression of Liaohe Basin. *J. Appl. Geophys.* **2021**, *195*, 104480. [CrossRef]
16. Puskarczyk, E. Applying of the Artificial Neural Networks (ANN) to Identify and Characterize *Sweet Spots* in Shale Gas Formations. *E3S Web Conf.* **2018**, *35*, 03008. [CrossRef]
17. Ren, X.; Hou, J.; Song, S.; Liu, Y.; Chen, D.; Wang, X.; Dou, L. Lithology Identification Using Well Logs: A Method by Integrating Artificial Neural Networks and Sedimentary Patterns. *J. Pet. Sci. Eng.* **2019**, *182*, 106336. [CrossRef]
18. Liu, X.Y.; Zhou, L.; Chen, X.H.; Li, J.Y. Lithofacies Identification Using Support Vector Machine Based on Local Deep Multi-Kernel Learning. *Pet. Sci.* **2020**, *17*, 954–966. [CrossRef]
19. Bressan, T.S.; Kehl de Souza, M.; Girelli, T.J.; Junior, F.C. Evaluation of Machine Learning Methods for Lithology Classification Using Geophysical Data. *Comput. Geosci.* **2020**, *139*, 104475. [CrossRef]
20. Duan, Y.; Xie, J.; Su, Y.; Liang, H.; Hu, X.; Wang, Q.; Pan, Z. Application of the Decision Tree Method to Lithology Identification of Volcanic Rocks-Taking the Mesozoic in the Laizhouwan Sag as an Example. *Sci. Rep.* **2020**, *10*, 19209. [CrossRef] [PubMed]
21. Liu, J.; Tian, F.; Zhao, A.; Zheng, W.; Cao, W. Logging Lithology Discrimination with Enhanced Sampling Methods for Imbalance Sample Conditions. *Appl. Sci.* **2024**, *14*, 6534. [CrossRef]
22. Chen, J.; Deng, X.; Shan, X.; Feng, Z.; Zhao, L.; Zong, X.; Feng, C. Intelligent Classification of Volcanic Rocks Based on Honey Badger Optimization Algorithm Enhanced Extreme Gradient Boosting Tree Model: A Case Study of Hongche Fault Zone in Junggar Basin. *Processes* **2024**, *12*, 285. [CrossRef]
23. Ali, M.; Zhu, P.; Huolin, M.; Jiang, R.; Zhang, H.; Ashraf, U.; Hussain, W. Data-Driven Machine Learning Approaches for Precise Lithofacies Identification in Complex Geological Environments. *Geo-Spat. Inf. Sci.* **2024**, 1–21. [CrossRef]
24. Wang, C.; Li, P.; Long, Q.; Chen, H.; Wang, P.; Meng, Z.; Wang, X.; Zhou, Y. Deep Learning for Refined Lithology Identification of Sandstone Microscopic Images. *Minerals* **2024**, *14*, 275. [CrossRef]
25. Wu, L.; Dong, Z.; Li, W.; Jing, C.; Qu, B. Well-Logging Prediction Based on Hybrid Neural Network Model. *Energies* **2021**, *14*, 8583. [CrossRef]

26. Pan, L.; Gao, J.; Yang, Y.; Wang, Z.; Gao, Z. Automatic Seismic Lithology Interpretation via Multiattribute Integrated Deep Learning. *IEEE Geosci. Remote Sens. Lett.* **2023**, *20*, 7503205. [CrossRef]
27. Li, Z.; Deng, S.; Hong, Y.; Wei, Z.; Cai, L. A Novel Hybrid CNN–SVM Method for Lithology Identification in Shale Reservoirs Based on Logging Measurements. *J. Appl. Geophys.* **2024**, *223*, 105346. [CrossRef]
28. Fu, D.; Su, C.; Wang, W.; Yuan, R. Deep Learning Based Lithology Classification of Drill Core Images. *PLoS ONE* **2022**, *17*, e0270826. [CrossRef]
29. Mousavi, S.H.R.; Hosseini-Nasab, S.M. Residual Convolutional Neural Network for Lithology Classification: A Case Study of an Iranian Gas Field. *Int. J. Energy Res.* **2024**, *2024*, 5576859. [CrossRef]
30. He, Y.; Li, W.; Dong, Z.; Zhang, T.; Shi, Q.; Wang, L.; Wu, L.; Qian, S.; Wang, Z.; Liu, Z.; et al. Lithologic Identification of Complex Reservoir Based on PSO-LSTM-FCN Algorithm. *Energies* **2023**, *16*, 2135. [CrossRef]
31. Liu, Y.; Zhang, Y.; Mao, X.; Zhou, X.; Chang, J.; Wang, W.; Wang, P.; Qi, L. Lithological Facies Classification Using Attention-Based Gated Recurrent Unit. *Tsinghua Sci. Technol.* **2024**, *29*, 1206–1218. [CrossRef]
32. Imamverdiyev, Y.; Sukhostat, L. Lithological Facies Classification Using Deep Convolutional Neural Network. *J. Pet. Sci. Eng.* **2019**, *174*, 216–228. [CrossRef]
33. Venkateshwaran, B.; Ramkumar, Mu.; Siddiqui, N.A.; Haque, A.E.; Sugavanam, G.; Manobalaji, A. A Graph Convolutional Network Approach to Qualitative Classification of Hydrocarbon Zones Using Petrophysical Properties in Well Logs. *Nat. Resour. Res.* **2024**, *33*, 637–664. [CrossRef]
34. Lu, G.; Zeng, L.; Dong, S.; Huang, L.; Liu, G.; Ostadhassan, M.; He, W.; Du, X.; Bao, C. Lithology Identification Using Graph Neural Network in Continental Shale Oil Reservoirs: A Case Study in Mahu Sag, Junggar Basin, Western China. *Mar. Pet. Geol.* **2023**, *150*, 106168. [CrossRef]
35. Yuan, C.; Wu, Y.; Li, Z.; Zhou, H.; Chen, S.; Kang, Y. Lithology Identification by Adaptive Feature Aggregation under Scarce Labels. *J. Pet. Sci. Eng.* **2022**, *215*, 110540. [CrossRef]
36. Zhao, F.; Zhou, Z.; Zhai, H.; Zhang, P.; Li, X. ResGAT: A Residual Graph Attention Network for Lithology Identification. *IEEE Geosci. Remote Sens. Lett.* **2025**, *22*, 7500605. [CrossRef]
37. Sun, Y.; Pang, S.; Zhang, Y. Enhancing Fluid Identification via an Innovative Transformer Model with Bidirectional Recurrent Units Network Leveraging Well Logging Data. *Phys. Fluids* **2024**, *36*, 76626. [CrossRef]
38. Singh, D.; Singh, B. Investigating the Impact of Data Normalization on Classification Performance. *Appl. Soft Comput.* **2020**, *97*, 105524. [CrossRef]
39. Huang, L.; Qin, J.; Zhou, Y.; Zhu, F.; Liu, L.; Shao, L. Normalization Techniques in Training DNNs: Methodology, Analysis and Application. *IEEE Trans. Pattern Anal. Mach. Intell.* **2023**, *45*, 10173–10196. [CrossRef]
40. Wang, Z.; Xie, K.; Wen, C.; Sheng, G.; He, J.; Tian, H. Multi-Scale Spatiotemporal Feature Lithology Identification Method Based on Split-Frequency Weighted Reconstruction. *Geoenergy Sci. Eng.* **2023**, *226*, 211794. [CrossRef]
41. Veličković, P.; Cucurull, G.; Casanova, A.; Romero, A.; Liò, P.; Bengio, Y. Graph Attention Networks. *arXiv* **2018**, arXiv:1710.10903.
42. Yin, X.; Wu, G.; Wei, J.; Shen, Y.; Qi, H.; Yin, B. Multi-Stage Attention Spatial-Temporal Graph Networks for Traffic Prediction. *Neurocomputing* **2021**, *428*, 42–53. [CrossRef]
43. Chen, P.Y.; Yu, H.M. Euclidean Distance-Based Method for Variable Selection and Its Application in Geological Data. *J. Interdiscip. Math.* **2016**, *19*, 215–232. [CrossRef]
44. Han, K.; Wang, Y.; Chen, H.; Chen, X.; Guo, J.; Liu, Z.; Tang, Y.; Xiao, A.; Xu, C.; Xu, Y.; et al. A Survey on Vision Transformer. *IEEE Trans. Pattern Anal. Mach. Intell.* **2023**, *45*, 87–110. [CrossRef]
45. Lin, T.; Wang, Y.; Liu, X.; Qiu, X. A Survey of Transformers. *AI Open* **2022**, *3*, 111–132. [CrossRef]
46. Yale, D.P.; Jamieson, W.H. Static and Dynamic Rock Mechanical Properties in the Hugoton and Panoma Fields, Kansas. In Proceedings of the SPE Mid-Continent Gas Symposium, Amarillo TA, USA, 22–24 May 1994; OnePetro: Richardson, TX, USA, 1994. [CrossRef]